JCIM JOURNAL OF CHEMICAL INFORMATION AND MODELING

pubs.acs.org/jcim Article

# Promiscuous Esterases Counterintuitively Are Less Flexible than Specific Ones

Christina Nutschel, Cristina Coscolín, Benoit David, Daniel Mulnaes, Manuel Ferrer, Karl-Erich Jaeger, and Holger Gohlke*

Cite This: J. Chem. Inf. Model. 2021, 61, 2383−2395 Read Online

ACCESS | Metrics & More | Article Recommendations | Supporting Information

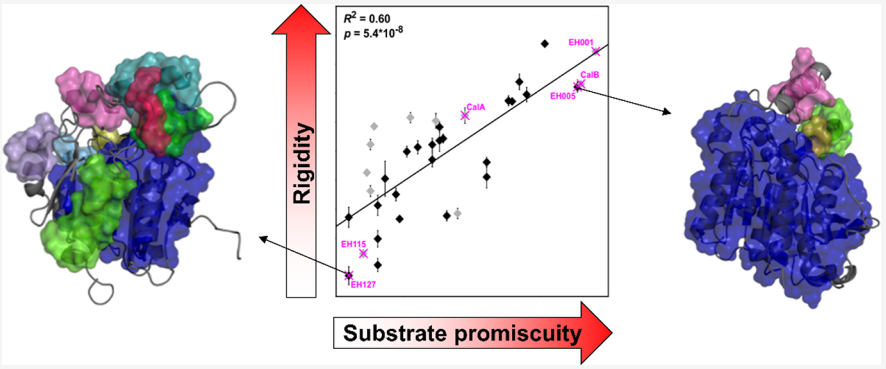


**ABSTRACT:** Understanding mechanisms of promiscuity is increasingly important from a fundamental and application point of view. As to enzyme structural dynamics, more promiscuous enzymes generally have been recognized to also be more flexible. However, examples for the opposite received much less attention. Here, we exploit comprehensive experimental information on the substrate promiscuity of 147 esterases tested against 96 esters together with computationally efficient rigidity analyses to understand the molecular origin of the observed promiscuity range. Unexpectedly, our data reveal that promiscuous esterases are significantly less flexible than specific ones, are significantly more thermostable, and have a significantly increased specific activity. These results may be reconciled with a model according to which structural flexibility in the case of specific esterases serves for conformational proofreading. Our results signify that an esterase sequence space can be screened by rigidity analyses for promiscuous esterases as starting points for further exploration in biotechnology and synthetic chemistry.



## 1. INTRODUCTION

Enzymes involved in primary metabolism typically exquisitely discriminate against other metabolites. Nevertheless, evolution of specificity is only pushed by nature to the point at which "unauthorized" reactions do not impair the fitness of the organism.[1] As a result, the universe of promiscuous activities available in nature has been suggested to be enormous.[2,3] Understanding mechanisms of promiscuity has thus become increasingly important for the fundamental understanding of molecular recognition and how enzyme function has evolved over time[4] but also to optimize enzyme engineering applications.[5−7] A particular challenge in the latter case is the ability to discover a suitable enzyme with "sufficient" promiscuous activity to serve as a starting point for further exploration.[1]

Enzyme structural dynamics, besides its role in catalysis[8,9] and allosteric regulation,[10−13] has been recognized as an important mechanism by which promiscuity can be achieved.[5] Prominent examples are human cytochrome P450 (CYP) enzymes, for which crystallographic studies and molecular simulations demonstrated that more promiscuous CYPs show larger structural plasticity and mobility,[14−16] or TEM-1 $\beta$-lactamase and a resurrected progenitor, for which molecular simulations show that the pocket of the ancestral, and more promiscuous, enzyme fluctuates to a greater extent.[17] However, examples for the opposite, i.e., conformational changes selected in evolution such that they enhance specificity in molecular recognition,[18] have received much less attention in the context of enzyme promiscuity.

A clear limitation for scrutinizing the link between enzyme structural dynamics and substrate promiscuity is the general lack of large-scale data on one enzyme (super)family tested against a multitude of ligands[19] (cf. ref[1] for notable

Received: February 9, 2021
Published: May 5, 2021




https://doi.org/10.1021/acs.jcim.1c00152
J. Chem. Inf. Model. 2021, 61, 2383−2395

exceptions). Likewise, acquiring information on enzyme dynamics at the atomistic level by experimental techniques or classical molecular dynamics (MD) simulations is burdensome. Here, we exploit comprehensive experimental information on the substrate promiscuity[20] of esterases (abbreviated EHs, for "ester hydrolases")[21] together with computationally efficient rigidity analyses[22−25] of comparative models of EHs to understand the molecular origin of the observed promiscuity range. Enzyme rigidity, or its opposite flexibility, is a static property that denotes the impossibility, or possibility, of motions in an enzyme under force without giving information about directions and magnitudes of movements.[25] Thus, enzyme flexibility should not be confused with enzyme mobility, which describes actual motions in an enzyme. Rigidity analysis results do not rely on the accurate description of the time dependency of processes,[25] which makes them valuable in cases where timescales over multiple orders of magnitude may govern such processes, like in enzyme dynamics.[8,9]

In recent years, EHs have obtained much attention in basic research and industrial applications.[26] EHs are widely distributed in nature within microbial communities (at least one EH is found in each bacterial genome), and they have been extensively examined with state-of-the-art (meta)genomic techniques and investigated by functional screenings compared to many other classes of enzymes. They also possess outstanding properties in terms of stability, reactivity, and scalability, making them appropriate biocatalysts to improve competitiveness, innovation capacity, and sustainability in a modern circular bio-economy.[27] Recently, a large-scale study on substrate promiscuity ($P_{EH}$, which denotes the number of esters hydrolyzed by an EH) of 147 phylogenetically, environmentally, and structurally diverse microbial EHs was described by Martínez-Martínez *et al.*,[21] in which all EHs were functionally assessed against a customized library of 96 esters. As to mechanistic understanding, the authors related $P_{EH}$ to a structural parameter, the active site effective volume. However, the impact of enzyme flexibility on $P_{EH}$ was not assessed.

In our study, we thus ask the following questions: (I) What is the relation between $P_{EH}$ and EH flexibility? (II) Does this relation hold if experimentally determined EH thermostabilities are used as proxies for enzyme flexibility? (III) What is the relation between $P_{EH}$ and EHs' specific activities? (IV) Is there a preference of promiscuous or specific EHs for a particular type of esters? (V) Can this preference be understood with respect to EH flexibilities?

We addressed these questions by exploiting comprehensive experimental information on the substrate promiscuity of esterases tested against 96 esters together with computationally efficient rigidity analyses to understand the molecular origin of the observed promiscuity range. Unexpectedly, our data reveal that promiscuous esterases are significantly less flexible than specific ones, are significantly more thermostable, and have a significantly increased specific activity.

## 2. MATERIALS AND METHODS

**2.1. Definition of Data Sets.** The present study builds on the study from Martínez-Martínez *et al.*[21] To assess $P_{EH}$, i.e., the number of esters hydrolyzed by an EH irrespective of the catalytic efficiency, the authors experimentally investigated 147 phylogenetically, environmentally, and structurally diverse microbial EHs (termed experimental data set) against a customized library of 96 different esters. Two commercial lipases, which have found wide biotechnological applications, CalA and CalB from *Pseudozyma aphidis* (formerly *Candida antarctica*), were included for comparison. For details on determining and classifying $P_{EH}$, see the Supporting Information. To validate that $P_{EH}$ defines promiscuity of EHs in a quantitative manner, $k_{cat}$ and $K_m$ values were determined for 10 expressed and purified EHs covering the entire $P_{EH}$ range (see Section 2.9) and a promiscuity index $I$ (see eq S4, Supporting Information) computed and compared to $P_{EH}$. Finally, the similarity of the ester substrates was assessed by the maximum pairwise Tanimoto-Combo similarity score $\delta_{ij}$ for compound $i$ versus $j$, accounting for shape and chemical complementary between 3D structures, and the mean maximum pairwise Tanimoto-Combo similarity score $\delta_i$ of a substrate $i$ to all other substrates in the data set (see the Supporting Information).

As our computational approach involves extensive molecular dynamic (MD) simulations for generating conformational ensembles (see Section 2.3), we selected 35 EHs from the volume data set (termed flexibility data set) for comparative modeling (see Section 2.2). The criteria for choosing EHs of the flexibility data set are explained in Section 3.1.

**2.2. Comparative Modeling and Validations of the Flexibility Data Set.** Comparative models of the flexibility data set (see Section 2.1) were generated using our in-house structure prediction meta-tool TopModel[28] that has been successfully applied in previous studies.[29−32] TopModel uses multiple state-of-the-art threading and sequence/structure alignment tools to generate a large ensemble of models from different pairwise and multiple alignments of the top five highest-ranked template structures. The TopModel software is available at https://cpclab.uni-duesseldorf.de/index.php/Software.

The quality of the comparative models was assessed by our meta Model Quality Assessment Program (meta-MQAP) TopScore.[33] TopScore uses deep neural networks (DNN) to combine scores from 15 different primary MQAPs to predict accurate residue-wise and whole-protein error estimates. For details on the model quality assessment by TopScore and validation, see the Supporting Information.

To test whether the catalytically active residues (CARs) of the comparative models are accessible for substrates, we applied the CAVER 3.0.3 PyMOL Plugin.[34] Starting points for the computations were defined based on the Cartesian coordinates of the CARs' center of mass (COM). Default values were used for the probe radius (0.9 Å), shell radius (3.0 Å), and shell depth (4.0 Å).

**2.3. Generation of Structural Ensembles.** Structural ensembles of EHs were generated by all-atom MD simulations of, in total, 5 $\mu$s simulation time per EH. For details on starting structure preparation, parameterization, and equilibration, see the Supporting Information.

All minimization, equilibration, and production simulations were performed with the pmemd.cuda module[35] of Amber19.[36] During production simulations, we set the time step to integrate Newton's equation of motion to 4 fs following the hydrogen mass repartitioning strategy.[37] Coordinates were stored into a trajectory file every 200 ps. This resulted in 5000 configurations for each production run that were considered for subsequent analyses.

**2.4. Constraint Network Analysis.** The flexibility analyses were performed with the Constraint Network Analysis (CNA) software package (version 3.0).[22−25] CNA functions as



https://doi.org/10.1021/acs.jcim.1c00152
J. Chem. Inf. Model. 2021, 61, 2383−2395

a front-end and back-end to graph theory-based software Floppy Inclusions and Rigid Substructure Topography (FIRST).[38] Applying CNA to biomolecules aims at identifying their composition of rigid clusters and flexible regions, which can aid in the understanding of the biomolecular structure, stability, and function.[23−25] As the mechanical heterogeneity of biomolecular structures is intimately linked to their diverse biological functions, biomolecules generally show a hierarchy of rigidity and flexibility.[22] In CNA, biomolecules are modeled as constraint networks in a body-and-bar representation, which has been described in detail by Hesphenheide *et al.*[39] A fast combinatorial algorithm, the pebble game, counts the bond rotational degrees of freedom and floppy modes (internal, independent degrees of freedom) in the constraint network.[40] To monitor the hierarchy of rigidity and flexibility of biomolecules, CNA performs thermal unfolding simulations by consecutively removing noncovalent constraints (hydrogen bonds, including salt bridges) from a network in increasing order of their strength.[41−43] For details on thermal unfolding simulations, see the Supporting Information. To improve the robustness and investigate the statistical uncertainty, we carried out CNA on ensembles of network topologies ($ENT^{MD}$) generated from MD trajectories (see Section 2.3).[44]

CNA software is available under academic license at https://cpclab.uni-duesseldorf.de/index.php/Software and the CNA web server is accessible at https://cpclab.uni-duesseldorf.de/cna.

**2.5. Local and Global Indices.** From the thermal unfolding simulations, CNA computes a comprehensive set of indices to quantify biologically relevant characteristics of the protein's stability. Global indices are used for determining the rigidity and flexibility at a macroscopic level; local indices determine the rigidity and flexibility at a microscopic level of bonds.[45] The cluster configuration entropy $H_{type2}$ is a global index that has been introduced by Radestock and Gohlke.[22] As done previously, we applied $H_{type2}$ as a measure for global structural stability of proteins.[22,43,46−50] The stability map $rc_{ij}$ is a local index that has been introduced by Radestock and Gohlke.[22] We applied $rc_{ij}$ as a measure for local structural stability of proteins in previous studies.[47,49,50] For details on both indices, see the Supporting Information.

**2.6. Root-Mean-Square Fluctuations.** The per-residue root-mean-square fluctuations were calculated for each EH ($RMSF_{EH}$) and for its CARS ($RMSF_{CAR}$) based on the MD trajectories (see Section 2.3). Prior to the calculations, the structures of each trajectory were superimposed onto the average structure using the 90% least mobile residues of the respective EHs.[51]

**2.7. Torsion Angles.** For each of the 96 esters, the number of freely rotatable bonds (torsion angles, TA) was calculated based on the SMILES codes provided by Martínez-Martínez *et al.*[21]

To compare how many esters with a specific TA are hydrolyzed by each EH, we calculated the normalized proportion of ester hydrolysis with a specific TA ($norm_{ester}(TA)$) as the number of hydrolyzed esters with a specific TA ($ester_{hydrolyzed}(TA)$) divided by the total number of esters in the data set with this specific TA ($ester_{library}(TA)$) (eq 1).

$$\mathrm{norm}_{\mathrm{ester}}(\mathrm{TA})\ [\%] = \frac{\mathrm{ester}_{\mathrm{hydrolyzed}}(\mathrm{TA})}{\mathrm{ester}_{\mathrm{library}}(\mathrm{TA})} \times 100\% \quad (1)$$

**2.8. Circular Dichroism Spectroscopy.** Eleven EHs, namely, $EH_1$ (Protein Data Bank (PDB) acc. no. 5JD4), $EH_2$ (GenBank acc. no. KY483643), $EH_3$ (GenBank acc. no. KY483645), $EH_4$ (GenBank acc. no. KR107250), $EH_6$ (GenBank acc. no. KP347751), $EH_8$ (GenBank acc. no. WP_011587341.1), $EH_9$ (GenBank acc. no. KY483648), $EH_{16}$ (GenBank acc. no. KP347759), $EH_{21}$ (GenBank acc. no. KP347760), $EH_{37}$ (GenBank acc. no. KR107248), and $EH_{43}$ (GenBank acc. no. KP347758) from metagenomic origin, were used in the present study to perform circular dichroism (CD) determinations. The vector pET46 Ek/LIC and the host *Escherichia coli* (*E. coli*) BL21(DE3) were the sources of the $His_6$-tag $EH_1$, $EH_4$, $EH_8$, and $EH_{37}$, the vector pBXNH3 and the host *E. coli* MC1061 were the sources of the $His_6$-tag $EH_2$, $EH_3$, and $EH_9$, and the vector p15Tv-L and the host *E. coli* BL21(DE3) were the sources of $EH_6$, $EH_{16}$, $EH_{21}$, and $EH_{43}$. Prior to analyses, the soluble His-tagged proteins were produced and purified after binding to a Ni-NTA His-Bind resin (Sigma-Aldrich, MO, US) as described by Martínez-Martínez *et al.*[21] Purity was assessed as >98% using SDS-PAGE analysis in a Mini PROTEAN electrophoresis system (Bio-Rad, Madrid, Spain) and subsequent staining with Coomassie Brilliant Blue. A total of about 10−20 mg of total purified recombinant protein was obtained on average from 1 L of culture. All proteins were stored at −20 °C at a concentration of 10 mg/mL in 40 mM (4-(2-hydroxyethyl)-1-piperazineethanesulfonic acid (HEPES) buffer (pH 7.0) until use. The CD spectra were acquired between 190 and 270 nm with a Jasco J-720 spectropolarimeter equipped with a Peltier temperature controller, employing a 0.1 mm cell at 25 °C. The spectra were analyzed, and denaturation temperatures were determined at 220 nm between 10 and 85 °C at a rate of 30 °C per hour in 40 mM HEPES buffer (pH 7.0). A protein concentration of 1.0 mg $mL^{-1}$ was used. Denaturation temperatures were calculated by fitting the ellipticity (mdeg) at 220 nm at each of the different temperatures using a five-parameter sigmoid fit with Sigma Plot 14.0. The CD data are available in CD Data Table.

**2.9. Kinetic Parameter Determination.** Ten EHs, namely, $EH_1$ (PDB acc. no. 5JD4), $EH_3$ (GenBank acc. no. KY483645), $EH_5$ (GenBank acc. no. KR107271), $EH_7$ (GenBank acc. no. KY483644), $EH_{12}$ (GenBank acc. no. KR107263), $EH_{17}$ (GenBank acc. no. KR107278), $EH_{37}$ (GenBank acc. no. KR107248), $EH_{102}$ (Protein Data Bank acc. no. 5JD3), $EH_{115}$ (GenBank acc. no. KR107274), and $EH_{127}$ (GenBank acc. no. KR107253) from metagenomic origin, were used in the present study to perform kinetic determinations ($k_{cat}$ and $K_m$). The vector pET46 Ek/LIC and the host *E. coli* MC1061 were the sources of the $His_6$-tag $EH_1$, $EH_5$, $EH_{12}$, $EH_{17}$, $EH_{37}$, $EH_{102}$, $EH_{115}$, and $EH_{127}$, the vector pBXNH3 and the host *E. coli* MC1061 were the sources of the $His_6$-tag $EH_3$, and the vector pBXCH and the host *E. coli* MC1061 were the sources of the $His_6$-tag $EH_7$. The soluble His-tagged proteins were produced and purified as described by Martínez-Martínez *et al.*[21] For details, see above.

The kinetic parameters were calculated at 550 nm using a continuous pH indicator (phenol red; $\varepsilon_{550\ nm}$ = 8450 $M^{-1}$ $cm^{-1}$) assay at 550 nm in 384-well plates as previously described.[52] Briefly, to 40 μL of 5 mM 4-(2-hydroxyethyl)-1-piperazinepropanesulfonic acid (EPPS) buffer (pH 8.0), 2 μL of a stock ester solution was added to achieve the desired concentration of each ester. Finally, 2 μL of stock protein solution was immediately added to each well, to achieve the


https://doi.org/10.1021/acs.jcim.1c00152
J. Chem. Inf. Model. 2021, 61, 2383−2395

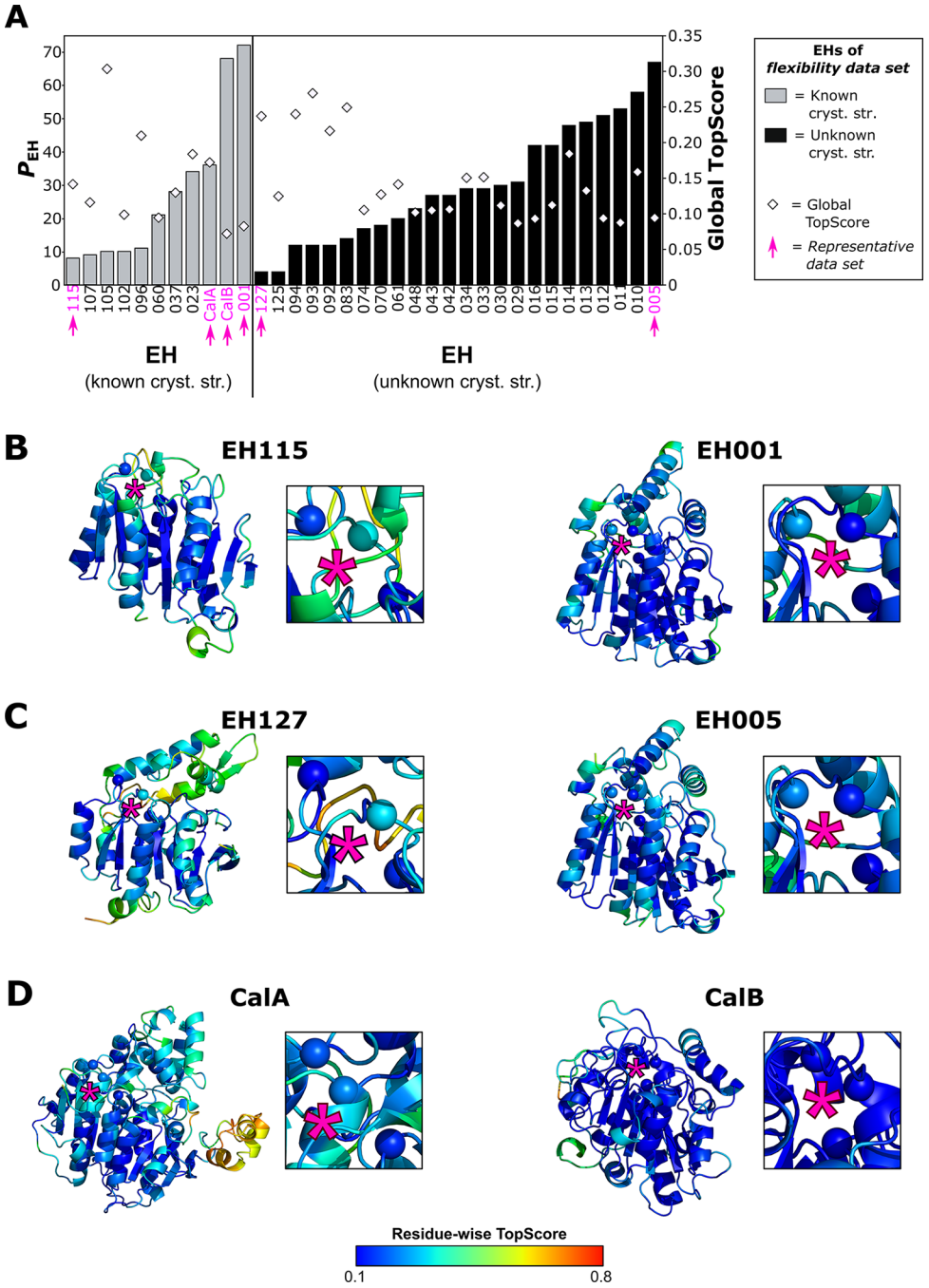


**Figure 1.** Comparative modeling of EHs. (A) Based on sequence data provided by a large-scale study from Martínez-Martínez *et al.*,[21] comparative models were generated for 35 EHs with known (left, 11 EHs) and unknown (right, 24 EHs) crystal structures using TopModel.[28] These EHs constitute the flexibility data set. The EHs vary in $P_{EH}$ (left ordinate, bars) and global TopScores (right ordinate, diamonds). Six EHs were selected as representatives of the flexibility data set (termed representative data set) as indicated by magenta arrows. The quality of the comparative models of (B) EHs with known crystal structures and lowest (EH115) or highest $P_{EH}$ (EH001), (C) EHs with unknown crystal structures and lowest (EH127) or highest $P_{EH}$ (EH005), and (D) commercial EHs with highest (CalA) or lowest $P_{EH}$ (CalB) was evaluated by TopScore.[33] For each comparative model, the residue-wise TopScore is shown: A good (bad) homology model shows a low (high) residue-wise TopScore (see color scale at the bottom). Insets depict CARs (spheres) within an EH. For clarity, the position of CARs is indicated by magenta stars.

desired protein concentration, using an Eppendorf Repeater M4 pipette (Eppendorf, Hamburg, Germany). The total reaction volume was 44 $\mu$L. Ester hydrolysis was measured at 30 °C in a Synergy HT Multi-Mode Microplate Reader in continuous mode at 550 nm over 24 h. One unit (U) of enzyme activity was defined as the amount of free enzyme or enzyme bound to the carrier required to transform 1 $\mu$mol of substrate in 1 min under the assay conditions using the reported extinction coefficient (phenol red at 550 nm = 8450 $M^{-1}$ $cm^{-1}$). For $K_m$ determination: [protein]: 4.5 $\mu$g $mL^{-1}$; [ester]: 0−100 mM; reaction volume: 44 $\mu$L; *T*: 30 °C; pH: 8.0. For $k_{cat}$ determination: [protein]: 0−270 $\mu$g $mL^{-1}$; [ester]: 100 mM; reaction volume: 44 $\mu$L; *T*: 30 °C; pH: 8.0. All values, in triplicates, were corrected for nonenzymatic transformation. Kinetic parameters were calculated by fitting


https://doi.org/10.1021/acs.jcim.1c00152
J. Chem. Inf. Model. 2021, 61, 2383−2395

the data with Sigma Plot 14.0. The kinetic parameters are available in Supplemental Data Table.

## 3. RESULTS

**3.1. Definition of Data Sets.** To understand the structural origin of and develop a method to predict $P_{EH}$, the present study builds on large-scale data from Martínez-Martínez *et al.*[21] The authors experimentally investigated $P_{EH}$ of 147 EHs (termed experimental data set; Figure S1) (see Section 2.1). In doing so, compromises needed to be made regarding the measurement of catalytic activity, i.e., specific activity was measured using enzymes expressed in *E. coli* without subsequent purification, only a single concentration of wet cells expressing enzymes (0.4 mg per ester) was used to measure activity, and the substrates were tested at a single concentration of circa 7 mM on average.[21] To validate that the $P_{EH}$ derived from the measured activities defines promiscuity of the enzymes in a quantitative manner, $k_{cat}$ and $K_m$ values were determined now for 10 expressed and purified EHs covering the entire $P_{EH}$ range (see Section 2.9). $k_{cat}/K_m$ ideally serves as the kinetic parameter in enzyme promiscuity studies for comparison.[53,54] From $k_{cat}/K_m$ values of an enzyme toward a defined set of substrates, a quantitative index of promiscuity $I$ (eq S4) can be calculated based on information entropy.[54] $I$ yields a very good and significant ($R^2$ = 0.79, $p$ = 0.0003) correlation with $P_{EH}$, indicating that $P_{EH}$ relates to EH promiscuity in a quantitative manner (Figure S2), although the range of $I$ suggests that large $P_{EH}$ may still be associated with moderate promiscuity. Note that although the $I$ is a functional parameter that is defined for a specified set of substrates, promiscuity indices for different enzymes are quantitatively comparable if they have been calculated using the same substrate set.[54] Furthermore, for the 10 EHs and using the colorimetric assay herein used, $k_{cat}/K_m$ can be measured with a standard error of the mean (SEM) as low as 0.05 $min^{-1}$ $mM^{-1}$, which corresponds to $k_{cat}$ and $K_m$ fitting values 2-fold above the background signals under assay conditions for each of the enzymes and esters. When $k_{cat}/K_m$ > 0.05 $min^{-1}$ $mM^{-1}$ is used as a criterion to define that a substrate is hydrolyzed, the resulting number of substrates for the 10 EHs yields an excellent and significant ($R^2$ = 0.99, $p < 10^{-4}$) correlation with $P_{EH}$ (Figure S3A), again indicating that $P_{EH}$ relates to EH promiscuity in a quantitative manner. Likewise, excellent and significant ($R^2$ = 0.97, $p < 10^{-4}$) correlations are obtained for $k_{cat}/K_m$ > 0.10, 0.50, and 1.00 $min^{-1}$ $mM^{-1}$ (Figure S3B−D). Finally, esters that are chemically similar to each other are expected to be metabolized similarly by an EH; such correlations in the substrate set would reduce the effective EH promiscuity. Therefore, similarity of the substrates was assessed by the maximum pairwise Tanimoto-Combo similarity score $\delta_{ij}$ for compound $i$ versus $j$, which is bounded between 0 for dissimilar compounds and 2 for identical ones, and the mean maximum pairwise Tanimoto-Combo similarity score $\delta_i$ of a substrate $i$ to all other substrates in the data set; the Tanimoto-Combo similarity score accounts for the shape and chemical complementary between 3D structures as determined by the Rapid Overlay of Chemical Structures approach.[55] Complete linkage clustering on the pairwise distance matrix calculated for all 96 compounds from $\delta_{ij}$ yielded 20 clusters at a distance of 1.0 (Figure S4), which is equivalent to $\delta_{ij}$ = 1.0, indicating that on average, less than five esters share a similarity that is half-way between dissimilar and identical. The negatively skewed histogram of $\delta_i$ furthermore shows that $\delta_i$ peaks at 1.0 and is below 1.2 (Figure S5), indicating that an ester generally shares a similarity to all other esters that is half-way between dissimilar and identical or worse.

Additionally, Martínez-Martínez *et al.* ranked (classified) $P_{EH}$ of 96 EHs (termed volume data set; Figure S1) based on the active site effective volume (see Section 2.1; eq S1),[21] which will be used here as a reference to compare the power of $P_{EH}$ predictions. As our computational approach involves extensive MD simulations for generating conformational ensembles, we selected 35 EHs from the volume data set based on the following criteria; they constitute the flexibility data set (Figure S1). (I) The data set contains all 11 EHs with known crystal structures (including the commercial EHs CalA and CalB) (Figure 1A and Table S1) and 24 EHs for which no experimental structure is available but for which comparative models can be generated (see Section 3.2; Figure 1A and Table S2). That way, we can probe to what extent the source of structural information influences the outcome of our results. (II) The chosen EHs of the data set show high diversities as to $P_{EH}$ and association to esterase families ($F_{EH}$, as defined by Arpigny and Jaeger[56]), similar to those found for the volume data set (Figures S6 and S7 and Tables S3 and S4). This resulted in $P_{EH}$ ranging from 4 to 72 (Figure 1A and Tables S1 and S2). In the following, we consider $P_{EH}$ as low if the EH hydrolyzes ≤9 esters (11% of the data set), as moderate if the EH hydrolyzes between 10 and 29 esters (49%), and as high if the EH hydrolyzes ≥30 esters (40%) (Figure S6 and Table S3). The data set covers 11 $F_{EH}$'s of which $F_{IV}$ (44% of the data set) and $F_V$ (21%) are the best represented ones (Figure S7 and Table S4). This reflects the proportion of their presence in the volume data set. (III) Only EHs with amino acid sequence identities ≥25% in comparison to an existing crystal structure were considered (see Section 2.1) to ensure a sufficient quality of generated comparative models.

Finally, to uniformly depict the results across the present study, six EHs were selected as representatives of the flexibility data set based on $P_{EH}$ (termed representative data set; Figure S1): EHs with the lowest (EH115) or highest $P_{EH}$ (EH001) and known crystal structures, EHs with the lowest (EH127) or highest $P_{EH}$ (EH005) and unknown crystal structures, and commercial EHs with the lowest (CalA) or highest $P_{EH}$ (CalB) (Figure 1A−D and Tables S1 and S2).

**3.2. Comparative Models of EHs Generated by TopModel Show an Overall and Residue-Wise Good Quality.** To generate structural models of EHs as starting points for our investigations, we performed template-based modeling of the flexibility data set using TopModel[28] (see Section 2.2). In doing so, we also generated comparative models of the 11 EHs for which crystal structures are available. These structural models will be used to judge the quality of the comparative modeling.

The quality of the comparative models of the flexibility data set was assessed with TopScore,[33] a meta Model Quality Assessment Program (meta-MQAP) (see Section 2.2). For the 11 EHs with a known crystal structure, the global TopScores range from 0.074 to 0.305 (Figure 1A and Table S1). As the global TopScore describes whole-protein error estimates, this shows that the structures contain between 7.4 and 30.5% errors. The high quality of the structures is also demonstrated by an average 1 − lDDT value of 0.22 ± 0.04 (SEM) computed from comparisons of the comparative models of EHs with a known crystal structure against these experimental



https://doi.org/10.1021/acs.jcim.1c00152
J. Chem. Inf. Model. 2021, 61, 2383−2395

reference structures (Table S5). lDDT is a superposition-free score that evaluates local distance differences of all atoms in a model. It was demonstrated that lDDT is well suited to assess local model quality, even in the presence of domain movements.[57] For reference, baseline 1 − lDDT values for models with threading errors are >0.65, and the 1 − lDDT value for random protein pairs is 0.80 ± 0.04.[57] For comparison, the average root-mean-square deviation between the models and the respective known crystal structures is 1.71 ± 0.29 Å (SEM) (Table S1). Notably, the global TopScore values well and significantly correlate ($R^2$ = 0.61, $p$ = 0.004) with the 1 − lDDT values, indicating that global TopScore values are well suited to assess the model quality of EHs (Figure S8 and Table S5). The global TopScore values of the comparative models of the other 24 EHs range from 0.087 to 0.269 (Figure 1A and Table S2), indicating that these models are of equal quality than the ones for EHs with a known crystal structure. The TopScore values of the representative data set lie in a comparable range (Figure 1A and Tables S1 and S2). Moreover, the comparative models of the flexibility data set show low residue-wise TopScore values,[33] indicating that all parts of a model are of good quality. We illustrate this for the residue-wise TopScore of the comparative models of the representative data set (Figure 1B−D). This also applies to structural regions around catalytically active residues (CARs) (Figure 1B−D). That way, it was possible to confirm CARs in models of EHs with known crystal structures and to unambiguously identify CARs in models of EHs with unknown crystal structures (Figure 1B−D and Tables S1 and S2).

Additionally, we validated that CARs in all models are accessible for substrates according to CAVER results[34] (see Section 2.2), i.e., that all models are in an open conformation: CARs are either located on the protein surface or are buried and connected with the surface by tunnels. We illustrate this for the comparative models of the representative data set (Figure S9).

To conclude, comparative models were generated for 35 EHs of the flexibility data set using TopModel. The models showed both an overall and residue-wise good structural quality. Additionally, we validated that CARs in all models are accessible for substrates.

### 3.3. Promiscuous EHs Are Globally Less Flexible.

Previous studies indicated that enzyme flexibility influences the substrate promiscuity of enzymes.[14−16] For gaining insights into how the flexibility of EHs is linked to $P_{EH}$, we applied CNA,[23,25] a rigidity theory-based approach to analyze biomolecular statics,[23−25] to the flexibility data set (see Section 2.4). To improve the robustness and investigate the statistical uncertainty, for each of the comparative models, we carried out CNA on ensembles of network topologies ($ENT^{MD}$) generated from five MD trajectories of 1 $\mu$s length each[46] (see Sections 2.3 and 2.4). To investigate if the global flexibility of the EHs influences $P_{EH}$, we predicted $T_p$, the phase transition temperature previously applied as a measure of structural stability of a protein,[22,43,46−50] for each EH (see Section 2.5). $T_p$ was averaged over five ensembles (see Sections 2.3 and 2.4), resulting in all but one case in SEM < 1.87 K (Figure 2A and Tables S1 and S2).

$T_p$ and $P_{EH}$ of the flexibility data set are well and significantly correlated ($R^2$ = 0.60, $p = 5.4 \times 10^{-8}$) (Figure 2A). To validate the consistency of our approach, we considered EHs with known or unknown crystal structures separately. In both cases, good and significant correlations between $T_p$ and $P_{EH}$ were

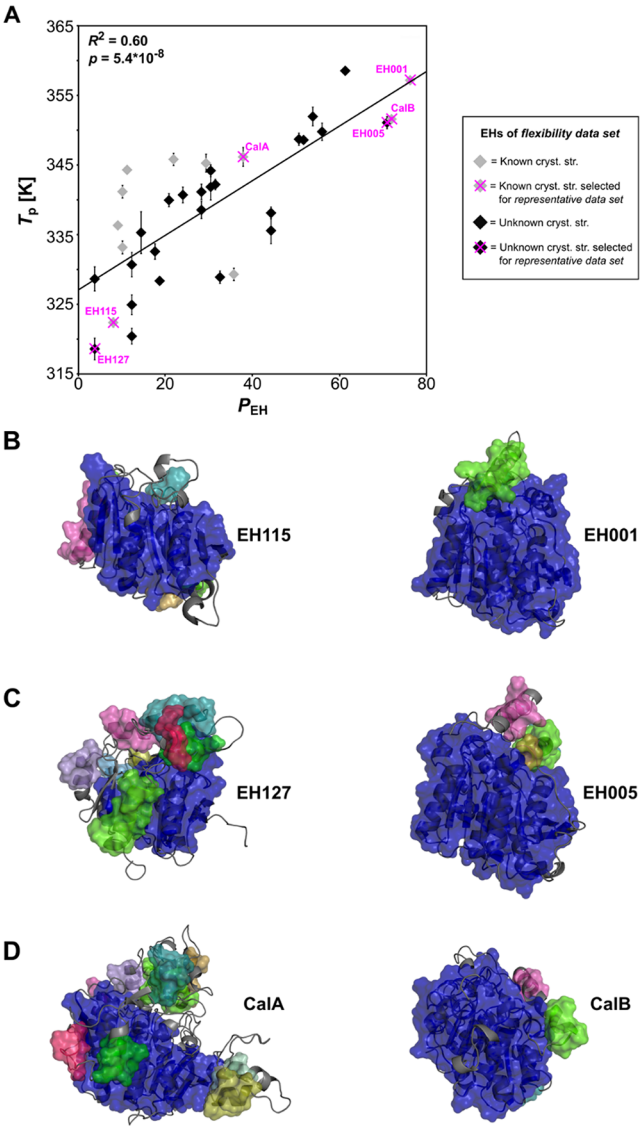


**Figure 2.** Correlation of $T_p$ *vs* $P_{EH}$. (A) Correlation between predicted $T_p$ based on the global index $H_{type2}$ and $P_{EH}$ for the flexibility data set. Data points colored gray (black) represent comparative models of EHs with (un)known crystal structures. The representative data set is indicated by magenta crosses. Error bars show the SEM over five independent MD simulations of 1 $\mu$s length each. Rigid cluster decomposition at 332 K during the thermal unfolding simulation of (B) EHs with known crystal structures and lowest (EH115) or highest $P_{EH}$ (EH001), (C) EHs with unknown crystal structures and lowest (EH127) or highest $P_{EH}$ (EH005), and (D) commercial EHs with lowest (CalA) or highest $P_{EH}$ (CalB). Rigid clusters are represented as uniformly colored blue, green, pink, cyan, and magenta bodies in the descending order of their sizes.

revealed (known crystal structures: $R^2$ = 0.48, $p$ = 0.019; unknown crystal structures: $R^2$ = 0.73, $p = 1.1 \times 10^{-7}$). The two $R^2$ values are not significantly different ($p$ = 0.33), which lends support to the quality of comparative models predicted with TopModel and indicates that future predictions on EHs with unknown experimental structures should be promising. Notably, EHs with high $P_{EH}$ have a high $T_p$ and *vice versa*, i.e., promiscuous EHs are globally less flexible. Exemplarily, this is depicted for EHs of the representative data set with known crystal structures and lowest (EH115) or highest $P_{EH}$ (EH001), which showed $T_p$ of 322.3 and 357.2 K, with


https://doi.org/10.1021/acs.jcim.1c00152
J. Chem. Inf. Model. 2021, 61, 2383−2395

unknown crystal structures and lowest (EH127) or highest $P_{EH}$ (EH005), which showed $T_p$ of 318.6 and 351.1 K, and with CalA and CalB, which showed $T_p$ of 346.2 and 351.6 K (Figure 2A and Tables S1 and S2). The differences in global structural stability of these EHs are illustrated by the rigid cluster decomposition at 332 K during the thermal unfolding simulations (Figure 2B−D): promiscuous EHs are globally more structurally stable at the elevated temperature as indicated by fewer, but larger, rigid clusters. Note that we used all EHs in the monomeric state to treat crystal structures and comparative models alike, although for some crystal structures, the biological assembly is a dimer or tetramer (Table S1). However, visual inspection revealed that in no case is the active site close to an interface. Furthermore, the $T_p$ values of respective monomeric and multimeric EHs show an absolute deviation of 3.5 ± 0.7 K (mean ± SEM) (Table S1), which is less than 2-fold the SEM of $T_p$ computations, indicating that the influence of the multimeric state on $T_p$ is negligible in these cases.

The EH flexibility analyzed so far is a static property and describes the potential of motions in a biomolecule.[25] Yet, direct information on mobility within EHs is available from the ensembles generated by MD simulations. We thus computed exemplarily $RMSF_{EH}$, a measure for protein mobility (see Section 2.6), across the ensembles of EHs from the representative data set. $RMSF_{EH}$, averaged over all residues and all five MD trajectories, and $P_{EH}$ do not yield a significant correlation ($p = 0.13$) (Figure S10A and Table S6), in contrast to $T_p$ and $P_{EH}$ ($R^2 = 0.93$, $p = 1.8 \times 10^{-3}$) (Figure S10B and Table S6). Still, as promiscuous EHs are globally less mobile, the same trend is obtained as in the case of the flexibility analysis.

To conclude, a good and significant correlation between $T_p$ and $P_{EH}$ was found for the flexibility data set ($R^2 = 0.60$, $p = 5.4 \times 10^{-8}$). These findings demonstrate that promiscuous EHs are globally less flexible. $RMSF_{EH}$ is less predictive for $P_{EH}$, although again, promiscuous EHs are characterized by a lower global mobility, mutually confirming either result.

**3.4. Promiscuous EHs Are More Thermostable.** Previous studies indicated that thermodynamically more thermostable proteins frequently have a higher structural stability.[47,50] To investigate if promiscuous EHs, which were predicted to be less flexible (see Section 3.3), are also more thermostable, CD spectroscopy was applied to determine the melting temperature $T_d$ of the EHs (see Section 2.8). Note that only if the unfolding of a protein is reversible, CD spectroscopy provides true thermodynamic properties.[58] However, even if the unfolding is irreversible, because the protein aggregates at high temperatures, the method can still give information about relative stabilities.[58] Hence, to reduce the potential impact of different aggregation kinetics of structurally different proteins, we applied CD spectroscopy to one $F_{EH}$ family only. In particular, we used $F_{IV}$ because it is the largest $F_{EH}$ (Table S7). As shown exemplarily in the CD spectrum for $T_d$ determination for EH001 (Figure 3A) and in CD Data Table for all other EHs listed in Table S7, only single-state transitions between totally folded and unfolded forms were observed, indicating that a bias due to possible different aggregation kinetics can be excluded. For each EH, $T_d$ determination was performed in triplicates with STD < 0.62 K. $T_d$ and $P_{EH}$ yield a fair and significant correlation ($R^2 = 0.32$, $p = 0.033$, Figure 3B; a similarly fair and significant correlation is found if the data point with the highest $T_d$ is omitted ($R^2 = 0.45$, $p = 0.016$)).

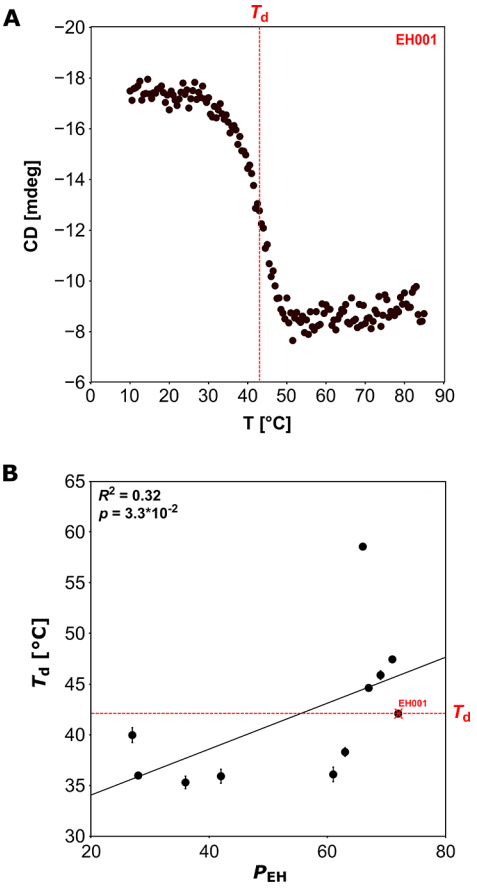


**Figure 3.** Determination of $T_d$ via CD spectroscopy. (A) Exemplary CD spectrum of EH001. The ellipticity changes in mdeg at 220 nm were plotted against the temperature, resulting in a sigmoidal curve. The inflection point was used to obtain the $T_d$ value (dotted line). (B) Correlation between $T_d$ and $P_{EH}$ for 11 EHs of $F_{IV}$.

To conclude, promiscuous EHs are not only globally less flexible but also more thermostable.

**3.5. Promiscuous EHs Have Less Flexible Catalytically Active Residues.** The good correlation of $P_{EH}$ and $T_p$ encouraged us to investigate if local flexibility characteristics of CARs will provide an even better predictor of EH promiscuity. We thus computed $Flex_{CAR}$ for the flexibility data set, i.e., the stability of rigid contacts between CARs and other residues that are at most 5 Å apart from each other, based on the local index $rc_{ij,neighbor}$ (see Section 2.5). For each EH, $Flex_{CAR}$ was averaged over five ensembles (see Sections 2.3 and 2.4), resulting in SEM < 0.06 kcal mol$^{-1}$ (Figure S11A and Tables S1 and S2).

$Flex_{CAR}$ and $P_{EH}$ of the flexibility data set yield a good and significant correlation ($R^2 = 0.51$, $p = 1.7 \times 10^{-6}$) (Figure S11A). To validate again the consistency of our approach, we considered EHs with known and unknown crystal structures separately. In both cases, good and significant correlations between $Flex_{CAR}$ and $P_{EH}$ were found (known crystal structures: $R^2 = 0.63$, $p = 3.7 \times 10^{-3}$; unknown crystal structures: $R^2 = 0.47$, $p = 2.2 \times 10^{-4}$), again lending support to the quality of comparative models predicted with TopModel. Hence, EHs with high $P_{EH}$ have low $Flex_{CAR}$ and *vice versa*, i.e., promiscuous EHs have less flexible CARs. Exemplarily, this is


https://doi.org/10.1021/acs.jcim.1c00152
J. Chem. Inf. Model. 2021, 61, 2383−2395

detailed for EHs of the representative data set with known crystal structures and lowest (EH115) or highest $P_{EH}$ (EH001), which showed $Flex_{CAR}$ values of −0.74 and −1.91 kcal mol$^{-1}$, with unknown crystal structures and lowest (EH127) or highest $P_{EH}$ (EH005), which showed $Flex_{CAR}$ values of −1.10 and −1.86 kcal mol$^{-1}$, and with CalA and CalB, which showed $Flex_{CAR}$ of −1.31 and −1.95 kcal mol$^{-1}$ (Figure S11A and Tables S1 and S2). The differences in local structural stability of these EHs are illustrated by rigid contacts between CARs and other residues that are at most 5 Å apart from each other (Figure S11B−D): promiscuous EHs are locally more structurally stable as indicated by more stable rigid contacts.

Finally, we exemplarily computed $RMSF_{CAR}$, a measure for the mobility of a protein's CARs (see Section 2.6), across the ensembles of EHs from the representative data set. Averaged $RMSF_{CAR}$ and $P_{EH}$ correlate worse ($R^2$ = 0.74, $p$ = 0.029) (Figure S12A and Table S6) than $Flex_{CAR}$ and $P_{EH}$ ($R^2$ = 0.92, $p = 2.4 \times 10^{-3}$) (Figure S12B and Table S6), paralleling the above results for the global measures. Still, again, as promiscuous EHs have less mobile CARs, the same trend is obtained as in the case of the flexibility analysis.

To conclude, a good and significant correlation between $Flex_{CAR}$ and $P_{EH}$ was found for the flexibility data set ($R^2$ = 0.51, $p = 1.7 \times 10^{-6}$). Hence, promiscuous EHs have less flexible CARs. $RMSF_{CAR}$ is less predictive for $P_{EH}$, although again, promiscuous EHs are characterized by less mobile CARs, mutually confirming either result.

**3.6. Promiscuous EHs Have an Increased Specific Activity.** In the study by Martínez-Martínez *et al.*,[21] the experimental data set was screened against 96 esters in a kinetic pH indicator assay (see Section 2.1). Besides the average specific activity $Act_{average}$ given in U/(g wet cells), also the average maximum specific activity $Act_{max}$ was determined. Motivated by the reactivity−selectivity principle (RSP) initially introduced for organic chemistry reactions,[59] which states that a more reactive chemical compound is less selective in chemical reactions, we intended to probe if $P_{EH}$ is related to $Act_{max}$. For this, we established an approximate linear free-energy relationship (LFER)[60] by relating $\log(Act_{max})$ and $\log(P_{EH})$ (Figure S13 and Table S8). In this analysis, the CalA and CalB preparations were excluded because $Act_{max}$ was given in U/(g total protein) there.

$\log(Act_{max})$ and $\log(P_{EH})$ of the experimental data set yield a good and significant correlation ($R^2$ = 0.50, $p = 4.6 \times 10^{-23}$) (Figure S13A). Likewise, $\log(Act_{max})$ and $\log(P_{EH})$ of the flexibility data set yield a fair and significant correlation ($R^2$ = 0.22, $p = 0.6 \times 10^{-2}$) (Figure S13B). To validate whether the same trend emerges for EHs with known and unknown crystal structures, we considered both types of EHs separately. In both cases, fair and significant correlations between $\log(Act_{max})$ and $\log(P_{EH})$ were found (known crystal structures: $R^2$ = 0.34, $p$ = 0.099; unknown crystal structures: $R^2$ = 0.23, $p$ = 0.019).

To conclude, good to fair and significant correlations between $\log(Act_{max})$ and $\log(P_{EH})$ of the experimental data set ($R^2$ = 0.50, $p = 4.6 \times 10^{-23}$) and the flexibility data set ($R^2$ = 0.22, $p = 0.6 \times 10^{-2}$) were found. Hence, promiscuous EHs have higher maximum specific activities.

**3.7. Specific EHs Prefer to Hydrolyze Large and Flexible Esters.** Next, we investigated which of the 96 esters was preferentially hydrolyzed by EHs with different $P_{EH}$'s. As a criterion, we chose the number of freely rotatable bonds of an ester, TA (see Section 2.7). We did so because TA is a combined measure for an ester's size and conformational dynamics.[61] To account for the uneven distribution of esters in our data set with respect to TA, we calculated $norm_{ester}(TA)$, i.e., the number of hydrolyzed esters with a specific TA ($ester_{hydrolyzed}(TA)$) divided by the total number of esters in the data set with this specific TA ($ester_{library}(TA)$) (see Section 2.7) (eq 1).

According to TA, the esters were classified into 17 groups that ranged from small esters with no rotatable bond to large esters with 56 rotatable bonds (Figure 4 and Table S9). Esters with three (24% of the ester library) and four (16% of the ester library) rotatable bonds are most frequent. The analysis of the experimental data set revealed that promiscuous EHs have high $norm_{ester}$ values irrespective of TA, i.e., promiscuous EHs accept a large variety of esters with different sizes and degrees of conformational dynamics (Figure 4A and Table S9). In contrast, specific EHs only have high $norm_{ester}$ values regarding esters with high TA, i.e., specific EHs preferentially hydrolyze (very) large and flexible esters (Figure 4A and Table S9). The same tendency was observed for the flexibility data set (Figure 4B and Table S9).

To conclude, promiscuous EHs accept a large variety of esters with different sizes and degrees of conformational dynamics, whereas specific EHs preferentially hydrolyze (very) large and flexible esters.

## 4. DISCUSSION

The main outcomes of our analyses are (I) that promiscuous EHs are significantly globally less flexible and have less flexible catalytically active residues than specific ones, (II) that promiscuous EHs are significantly more thermostable, (III) that promiscuous EHs have a significantly increased specific activity, and (IV) that specific EHs prefer to hydrolyze large and flexible esters.

We established these relations using one of the still few experimental large-scale data sets where a diverse set of EHs was functionally assessed against a customized library of dissimilar esters.[21] Functional promiscuity may arise from several conditions, including the environment of the enzyme or the concentration of a substrate, which may complicate the analysis of the molecular mechanism underlying promiscuity.[5] Still, functional promiscuity ultimately is a result of recognition promiscuity;[5] here, we therefore focused on substrate promiscuity,[20] i.e., an enzyme carries out its typical catalytic function using noncanonical substrates, in that experimental conditions had been kept constant for the assessment of the different esterase/ester combinations.[21] Almost all of the EHs were unambiguously assigned to one of the $F_{EH}$'s of the Arpigny and Jaeger classification, which is based mainly on a comparison of amino acid sequences.[56] Except for classes with a few members only (cyclase-like EHs and the yeast family), all other classes cover at least two of the three $P_{EH}$ ranges such that $P_{EH}$ cannot be assigned based on the EH's class affiliation (Figure S14 and Table S10) and, hence, amino acid sequence information. Even family $F_{IV}$, which contains a higher proportion of substrate-promiscuous EHs, also contains EHs with a small substrate range.

For scrutinizing the mechanism underlying esterase promiscuity at the atomistic level, we needed to apply comparative models of EHs, since only for ∼7% of the experimentally assessed EHs, crystal structures were available. Restricting the generation of esterase models to sequence identities ≥25% with respect to available targets yielded


https://doi.org/10.1021/acs.jcim.1c00152
J. Chem. Inf. Model. 2021, 61, 2383−2395

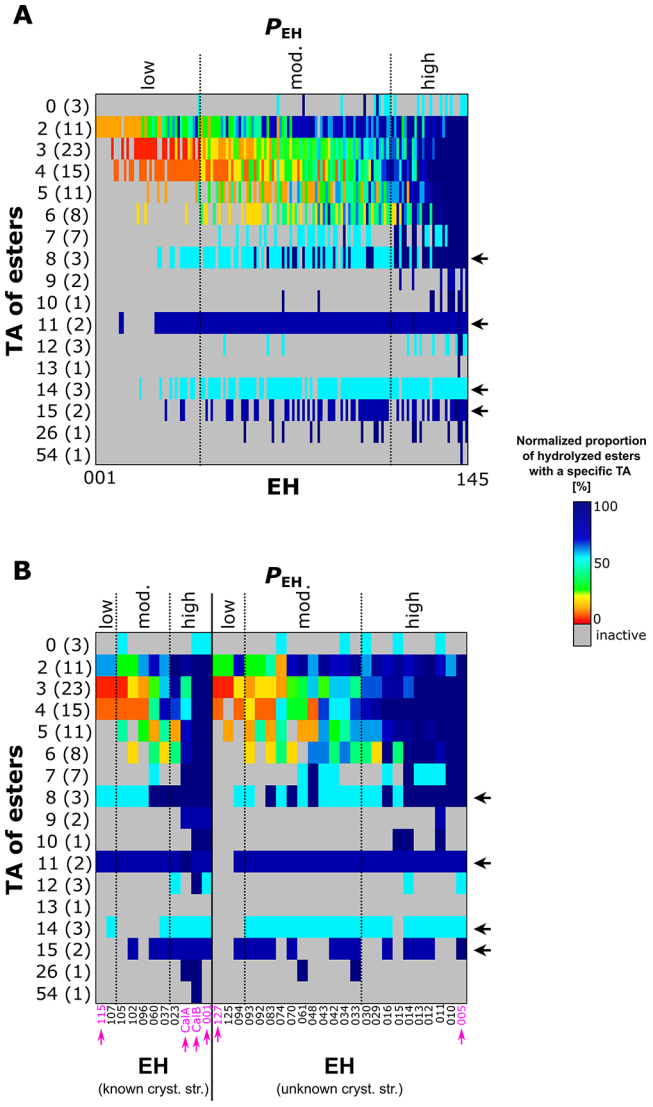


**Figure 4.** Relation between the number of esters' TA and $P_{EH}$. Relation between $norm_{ester}$, i.e., the relative proportion of the number of hydrolyzed esters with a specific TA, and $P_{EH}$ of (A) the experimental data set and (B) the flexibility data set containing EHs with known crystal structures (left), EHs with unknown crystal structures (right), and EHs constituting the representative data set (indicated by magenta arrows). TA was calculated based on SMILES codes of 96 esters provided by Martínez-Martínez *et al.*[21] A blue (red) color indicates that the EH hydrolyzes many (few) esters with a specific TA relative to the total number of esters in the data set with this specific TA (see color scale on the right); the total number of esters with a specific TA is given in brackets on the *y*-axis. $P_{EH}$ is defined as low if the EH hydrolyzes ≤9 esters, as moderate if the EH hydrolyzes between 10 and 29 esters, and as high if the EH hydrolyzes ≥30 esters.

generally good structural models both globally and locally, as also validated against cases where crystal structures are known. Throughout our study, we probed for the consistency of our analyses between subsets of EHs for which crystal structures are either known or not; we only found quantitative differences but no qualitative ones. One of the reasons is likely that rigidity analyses were based on structural ensembles generated by multiple and μs-long MD simulations, which has been shown to improve both global and local protein structures[62,63] to the level of approaching experimental accuracy[64] and markedly increases the robustness of the results.[44] We furthermore showed that results are consistent irrespective of whether EH flexibility characteristics were assessed globally or only for CARs and that mobility characteristics computed directly from MD trajectories show the same trend, although the correlation with $P_{EH}$ is insignificant. Finally, we used experimental melting temperatures of EHs as indicators for enzyme flexibility,[47,50] which yielded the same relation with $P_{EH}$ as computed flexibility characteristics. The partial use of comparative models rather than crystal structures throughout this study may lead to concern. Yet, our consistent and robust findings indicate that when applying this workflow to novel EHs, including to those for which no crystal structure exists but a structural homolog with a sequence identity ≥25%, it should be possible to discover enzymes with "sufficient" substrate promiscuity to serve as a starting point for further exploration in biotechnology and synthetic organic chemistry. In that respect, the flexibility characteristics of EHs analyzed here have a notably stronger predictive power than the active site effective volume introduced earlier[21] (Figure S15 and Tables S11 and S12). Still, besides flexibility, the size and architecture of the active site may be further determinants of catalytic promiscuity.[65]

The finding that promiscuous EHs are significantly globally less flexible and have less flexible catalytically active residues than specific EHs is in stark contrast to the general view of the role of structural flexibility for promiscuity:[4,5] Besides the examples of CYP and β-lactamase mentioned above, the possibility of dynamically restructuring active sites has also been recognized for other systems as underlying their promiscuity.[66−69] Finally, interactions between antibodies and antigens are a prominent example of the canonical relationship between flexibility and binding promiscuity: as antibodies mature to become more affine, their flexibility is decreased,[5] although in some cases, an initial increase in flexibility may be required for the evolution before subsequent mutations result in a rigidity increase.[70]

It has been recognized that conformational changes may not always be necessary for promiscuity if a variety of substrates can be bound by partial recognition or the presence of multiple binding sites.[5] However, these cases do not seem to be relevant reasons for EH promiscuity because partial recognition often is associated with catalytic inefficiency,[1] which is contrary to our observation that $P_{EH}$ correlates with EH activity, and the presence of multiple binding sites that could give rise to promiscuity is controverted by the finding that promiscuous EHs have large active site effective volumes,[21] i.e., large pockets with a few subpockets. Inversely, our findings of rigid promiscuous EHs may be consistent with the idea that multiple ligands can be accommodated in a single site by exploiting diverse interacting residues (Figure 5).

Our results as to specific but flexible EHs may be reconciled with a model according to which conformational changes may have been selected in EH evolution for their ability to enhance specificity in recognition (Figure 5), resulting in what has been termed conformational proofreading.[18] In the case of specific EHs, flexibility may help overcome a structural mismatch between the enzyme and its substrate existing when both are in their ground states, enhancing recognition specificity. This view is corroborated by our finding that specific EHs prefer to hydrolyze large and flexible substrates: Larger substrates can form more interactions with the enzyme, helping overcome the deformation energy required by the enzyme to optimizing the


https://doi.org/10.1021/acs.jcim.1c00152
J. Chem. Inf. Model. 2021, 61, 2383−2395

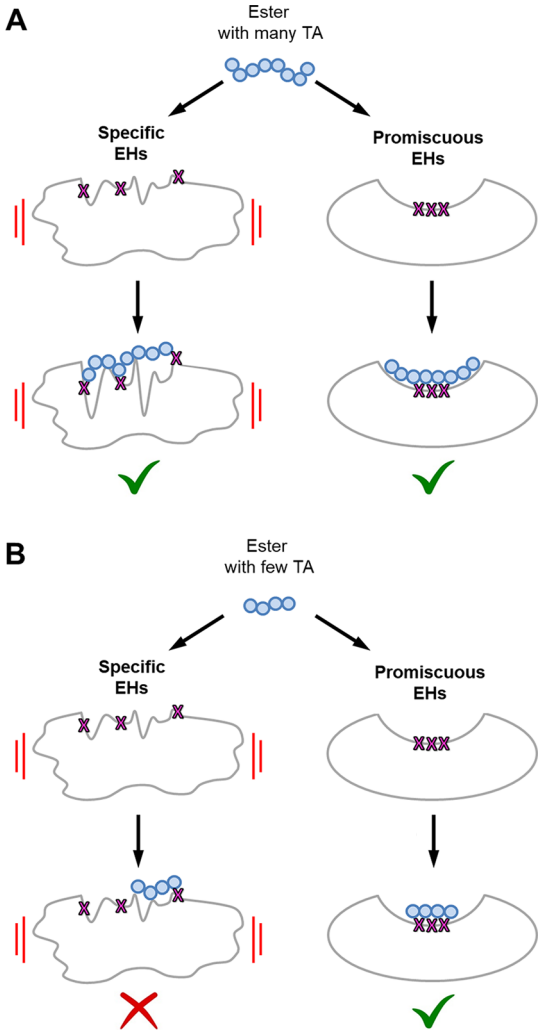


**Figure 5.** Mechanistic model of EH flexibility, ligand size, and conformational dynamics affecting $P_{EH}$. Impact of esters with (A) many or (B) few TA on specific, and hence more flexible (left), and promiscuous, and hence more rigid (right), EHs. Ligand parts connected by TA are represented as blue circles. Specific EHs and large ligands with many TA can mutually adapt (panel A, left), and promiscuous EH can bind large ligands (panel A, right) and small ligands (panel B, right) exploiting different interaction partners. Small (and/or rigid) ligands are not able to lead to a structural adaptation of specific EHs (panel B, left), though resulting in conformational proofreading. The red bars indicate the flexibility of the EHs. A green tick (red cross) indicates that ester cleavage is (not) catalyzed.

correct binding probability over the incorrect one; flexible substrates can tolerate higher strains and thus can be expected to participate in more binding events[71,72] (Figure 5). In that respect, the relation between structural flexibility of EHs and promiscuity found here is more causative than that between active site effective volume and promiscuity,[21] because small active site effective volumes found for specific EHs cannot rationalize why specific EHs prefer to hydrolyze large and flexible substrates.

In summary, the combined large-scale analysis of experimental EH promiscuity and computed EH flexibility reveals that promiscuous EHs are significantly less flexible than specific ones. This result is counterintuitive at first but may be reconciled with a model according to which multiple ligands can be accommodated in a single active site of promiscuous EHs by exploiting diverse interacting residues, whereas structural flexibility in the case of specific EHs serves for conformational proofreading. Our results furthermore signify that an EH sequence space, charted, e.g., by (meta)genomic studies, can be screened by rigidity analyses for promiscuous EHs that may serve as starting points for further exploration in biotechnology and synthetic organic chemistry.

## ■ ASSOCIATED CONTENT

### Supporting Information

The Supporting Information is available free of charge at https://pubs.acs.org/doi/10.1021/acs.jcim.1c00152.

Supplemental Materials and Methods, 12 supplemental tables, 14 supplemental figures, and supplemental references (PDF)

Kinetic data for 10 enzymes (XLSX)

CD data for 10 enzymes (XLSX)

## ■ AUTHOR INFORMATION


### Corresponding Author

**Holger Gohlke** − *John von Neumann Institute for Computing (NIC), Jülich Supercomputing Centre (JSC), Institute of Biological Information Processing (IBI-7: Structural Biochemistry), and Institute of Bio- and Geosciences (IBG-4: Bioinformatics), Forschungszentrum Jülich GmbH, 52425 Jülich, Germany; Institute for Pharmaceutical and Medicinal Chemistry, Heinrich Heine University Düsseldorf, 40225 Düsseldorf, Germany;* orcid.org/0000-0001-8613-1447; Phone: (+49) 2461-61-9711; Email: gohlke@uni-duesseldorf.de, h.gohlke@fz-juelich.de

### Authors

**Christina Nutschel** − *John von Neumann Institute for Computing (NIC), Jülich Supercomputing Centre (JSC), Institute of Biological Information Processing (IBI-7: Structural Biochemistry), and Institute of Bio- and Geosciences (IBG-4: Bioinformatics), Forschungszentrum Jülich GmbH, 52425 Jülich, Germany*

**Cristina Coscolín** − *Institute of Catalysis, Consejo Superior de Investigaciones Científicas, 28049 Madrid, Spain*

**Benoit David** − *Institute for Pharmaceutical and Medicinal Chemistry, Heinrich Heine University Düsseldorf, 40225 Düsseldorf, Germany*

**Daniel Mulnaes** − *Institute for Pharmaceutical and Medicinal Chemistry, Heinrich Heine University Düsseldorf, 40225 Düsseldorf, Germany*

**Manuel Ferrer** − *Institute of Catalysis, Consejo Superior de Investigaciones Científicas, 28049 Madrid, Spain;* orcid.org/0000-0003-4962-4714

**Karl-Erich Jaeger** − *Institute of Molecular Enzyme Technology, Heinrich Heine University Düsseldorf, 52425 Jülich, Germany; Institute of Bio- and Geosciences IBG-1: Biotechnology, Forschungszentrum Jülich GmbH, 52425 Jülich, Germany*

Complete contact information is available at: https://pubs.acs.org/10.1021/acs.jcim.1c00152


### Author Contributions

H.G. and K.-E.J. conceived the study. C.N. analyzed the experimental data, performed structure prediction, MD simulations and CNA computations, analyzed the computational data, and wrote the manuscript together with H.G. D.M.

initially contributed to the structure prediction. B.D. performed similarity analysis of esters. M.F. and C.C. measured and analyzed melting temperatures and determined kinetic parameters. H.G. supervised and managed the project. All authors reviewed and approved the manuscript.

### Notes

The authors declare no competing financial interest.

## ■ ACKNOWLEDGMENTS

C.N. is funded through a grant ("Vernetzungsdoktorand") provided by the Forschungszentrum Jülich. Parts of the study were supported by the German Federal Ministry of Education and Research (BMBF) through funding number 031B0837A "LipoBiocat" to H.G. and K.-E.J. and funding number 031L0182 "InCelluloProtStruct" to H.G., the German Research Foundation (DFG) through funding no. INST 208/704-1 FUGG to H.G., and INST 208/654-1 FUGG to K.-E.J., as well as the state of North Rhine Westphalia (NRW) and the European Regional Development Fund (EFRE) through funding no. 34-EFRE-0300096 "CLIB-Kompetenzzentrum Biotechnologie (CKB)" to H.G. and K.-E.J. H.G. is grateful for computational support and infrastructure provided by the "Zentrum für Informations- und Medientechnologie" (ZIM) at the Heinrich Heine University Düsseldorf. H.G. gratefully acknowledges the computing time granted by the John von Neumann Institute for Computing (NIC) and provided on the supercomputer JUWELS at Jülich Supercomputing Centre (JSC) (user IDs: HKF7; protil (project ID: 15956)).[73] H.G. is grateful to OpenEye for an academic license. M.F. and K.-E.J. acknowledge the grant "INMARE" from the European Union's Horizon 2020 (grant agreement no. 634486), M.F. the grants PCIN-2017-078 (within the Marine Biotechnology ERA-NET) and BIO2017-85522-R from the Ministerio de Economía, Industria y Competitividad, Agencia Estatal de Investigación (AEI), Fondo Europeo de Desarrollo Regional (FEDER), and European Union (EU), and the grant 2020AEP061 from the Agencia Estatal CSIC. C.C. thanks the Ministerio de Economía y Competitividad and FEDER for a Ph.D. fellowship (grant BES-2015-073829). The authors are grateful to David Almendral and Ruth Matesanz for their support of CD analysis. The funding sources had no involvement in the conduct of research or preparation of the article.

## ■ REFERENCES

(1) Copley, S. D. Shining a Light on Enzyme Promiscuity. *Curr. Opin. Struct. Biol.* **2017**, *47*, 167−175.
(2) Chen, R.; Gao, B.; Liu, X.; Ruan, F.; Zhang, Y.; Lou, J.; Feng, K.; Wunsch, C.; Li, S.-M.; Dai, J.; Sun, F. Molecular Insights into the Enzyme Promiscuity of an Aromatic Prenyltransferase. *Nat. Chem. Biol.* **2017**, *13*, 226−234.
(3) Huang, H.; Pandya, C.; Liu, C.; Al-Obaidi, N. F.; Wang, M.; Zheng, L.; Keating, S. T.; Aono, M.; Love, J. D.; Evans, B.; Seidel, R. D.; Hillerich, B. S.; Garforth, S. J.; Almo, S. C.; Mariano, P. S.; Dunaway-Mariano, D.; Allen, K. N.; Farelli, J. D. Panoramic View of a Superfamily of Phosphatases through Substrate Profiling. *Proc. Natl. Acad. Sci. U. S. A.* **2015**, *112*, E1974−E1983.
(4) Khersonsky, O.; Tawfik, D. S. Enzyme Promiscuity: A Mechanistic and Evolutionary Perspective. *Annu. Rev. Biochem.* **2010**, *79*, 471−505.
(5) Nobeli, I.; Favia, A. D.; Thornton, J. M. Protein Promiscuity and Its Implications for Biotechnology. *Nat. Biotechnol.* **2009**, *27*, 157−167.
(6) Mayer, C.; Dulson, C.; Reddem, E.; Thunnissen, A.-M. W. H.; Roelfes, G. Directed Evolution of a Designer Enzyme Featuring an Unnatural Catalytic Amino Acid. *Angew Chem Int Ed Engl* **2019**, *58*, 2083−2087.
(7) Leveson-Gower, R. B.; Mayer, C.; Roelfes, G. The Importance of Catalytic Promiscuity for Enzyme Design and Evolution. *Nat. Rev. Chem.* **2019**, *3*, 687−705.
(8) Eisenmesser, E. Z.; Bosco, D. A.; Akke, M.; Kern, D. Enzyme Dynamics During Catalysis. *Science* **2002**, *295*, 1520−1523.
(9) Henzler-Wildman, K. A.; Lei, M.; Thai, V.; Kerns, S. J.; Karplus, M.; Kern, D. A Hierarchy of Timescales in Protein Dynamics Is Linked to Enzyme Catalysis. *Nature* **2007**, *450*, 913−916.
(10) Holliday, M. J.; Camilloni, C.; Armstrong, G. S.; Vendruscolo, M.; Eisenmesser, E. Z. Networks of Dynamic Allostery Regulate Enzyme Function. *Structure* **2017**, *25*, 276−286.
(11) Goodey, N. M.; Benkovic, S. J. Allosteric Regulation and Catalysis Emerge Via a Common Route. *Nat. Chem. Biol.* **2008**, *4*, 474−482.
(12) Saavedra, H. G.; Wrabl, J. O.; Anderson, J. A.; Li, J.; Hilser, V. J. Dynamic Allostery Can Drive Cold Adaptation in Enzymes. *Nature* **2018**, *558*, 324−328.
(13) Tzeng, S. R.; Kalodimos, C. G. Protein Dynamics and Allostery: An Nmr View. *Curr. Opin. Struct. Biol.* **2011**, *21*, 62−67.
(14) Skopalík, J.; Anzenbacher, P.; Otyepka, M. Flexibility of Human Cytochromes P450: Molecular Dynamics Reveals Differences between Cyps 3a4, 2c9, and 2a6, Which Correlate with Their Substrate Preferences. *J. Phys. Chem. B.* **2008**, *112*, 8165−8173.
(15) Hendrychová, T.; Anzenbacherová, E.; Hudeček, J.; Skopalík, J.; Lange, R.; Hildebrandt, P.; Otyepka, M.; Anzenbacher, P. Flexibility of Human Cytochrome P450 Enzymes: Molecular Dynamics and Spectroscopy Reveal Important Function-Related Variations. *Biochim. Biophys. Acta* **2011**, *1814*, 58−68.
(16) Ekroos, M.; Sjögren, T. Structural Basis for Ligand Promiscuity in Cytochrome P450 3a4. *Proc. Natl. Acad. Sci. U. S. A.* **2006**, *103*, 13682−13687.
(17) Zou, T.; Risso, V. A.; Gavira, J. A.; Sanchez-Ruiz, J. M.; Ozkan, S. B. Evolution of Conformational Dynamics Determines the Conversion of a Promiscuous Generalist into a Specialist Enzyme. *Mol. Biol. Evol.* **2015**, *32*, 132−143.
(18) Savir, Y.; Tlusty, T. Conformational Proofreading: The Impact of Conformational Changes on the Specificity of Molecular Recognition. *PLoS One* **2007**, *2*, No. e468.
(19) Ferrer, M.; Martínez-Martínez, M.; Bargiela, R.; Streit, W. R.; Golyshina, O. V.; Golyshin, P. N. Estimating the Success of Enzyme Bioprospecting through Metagenomics: Current Status and Future Trends. *Microb. Biotechnol.* **2016**, *9*, 22−34.
(20) Hult, K.; Berglund, P. Enzyme Promiscuity: Mechanism and Applications. *Trends Biotechnol.* **2007**, *25*, 231−238.
(21) Martínez-Martínez, M.; Coscolín, C.; Santiago, G.; Chow, J.; Stogios, P. J.; Bargiela, R.; Gertler, C.; Navarro-Fernández, J.; Bollinger, A.; Thies, S.; Méndez-García, C.; Popovic, A.; Brown, G.; Chernikova, T. N.; García-Moyano, A.; Bjerga, G. E. K.; Pérez-García, P.; Hai, T.; Del Pozo, M. V.; Stokke, R.; Steen, I. H.; Cui, H.; Xu, X.; Nocek, B. P.; Alcaide, M.; Distaso, M.; Mesa, V.; Peláez, A. I.; Sánchez, J.; Buchholz, P. C. F.; Pleiss, J.; Fernández-Guerra, A.; Glöckner, F. O.; Golyshina, O. V.; Yakimov, M. M.; Savchenko, A.; Jaeger, K. E.; Yakunin, A. F.; Streit, W. R.; Golyshin, P. N.; Guallar, V.; Ferrer, M.; The Inmare Consortium. Determinants and Prediction of Esterase Substrate Promiscuity Patterns. *ACS Chem. Biol.* **2018**, *13*, 225−234.
(22) Radestock, S.; Gohlke, H. Exploiting the Link between Protein Rigidity and Thermostability for Data-Driven Protein Engineering. *Eng. Life Sci.* **2008**, *8*, 507−522.
(23) Pfleger, C.; Rathi, P. C.; Klein, D. L.; Radestock, S.; Gohlke, H. Constraint Network Analysis (Cna): A Python Software Package for Efficiently Linking Biomacromolecular Structure, Flexibility, (Thermo-) Stability, and Function. *J. Chem. Inf. Model.* **2013**, *53*, 1007−1015.


https://doi.org/10.1021/acs.jcim.1c00152
J. Chem. Inf. Model. 2021, 61, 2383−2395

(24) Krüger, D. M.; Rathi, P. C.; Pfleger, C.; Gohlke, H. Cna Web Server: Rigidity Theory-Based Thermal Unfolding Simulations of Proteins for Linking Structure,(Thermo-) Stability, and Function. *Nucleic Acids Res.* **2013**, *41*, W340−W348.
(25) Hermans, S. M. A.; Pfleger, C.; Nutschel, C.; Hanke, C. A.; Gohlke, H. Rigidity Theory for Biomolecules: Concepts, Software, and Applications. *Comput. Mol. Sci.* **2017**, *7*, No. e1311.
(26) de Godoy Daiha, K.; Angeli, R.; de Oliveira, S. D.; Almeida, R. V. Are Lipases Still Important Biocatalysts? A Study of Scientific Publications and Patents for Technological Forecasting. *PLoS One* **2015**, *10*, No. e0131624.
(27) Ferrer, M.; Bargiela, R.; Martínez-Martínez, M.; Mir, J.; Koch, R.; Golyshina, O. V.; Golyshin, P. N. Biodiversity for Biocatalysis: A Review of the $\alpha/\beta$-Hydrolase Fold Superfamily of Esterases-Lipases Discovered in Metagenomes. *Biocatal. Biotranfor.* **2015**, *33*, 235−249.
(28) Mulnaes, D.; Porta, N.; Clemens, R.; Apanasenko, I.; Reiners, J.; Gremer, L.; Neudecker, P.; Smits, S. H. J.; Gohlke, H. Topmodel: Template-Based Protein Structure Prediction at Low Sequence Identity Using Top-Down Consensus and Deep Neural Networks. *J. Chem. Theory Comput.* **2020**, *16*, 1953−1967.
(29) Gohlke, H.; Hergert, U.; Meyer, T.; Mulnaes, D.; Grieshaber, M. K.; Smits, S. H. J.; Schmitt, L. Binding Region of Alanopine Dehydrogenase Predicted by Unbiased Molecular Dynamics Simulations of Ligand Diffusion. *J. Chem. Inf. Model.* **2013**, *53*, 2493−2498.
(30) Widderich, N.; Pittelkow, M.; Höppner, A.; Mulnaes, D.; Buckel, W.; Gohlke, H.; Smits, S. H. J.; Bremer, E. Molecular Dynamics Simulations and Structure-Guided Mutagenesis Provide Insight into the Architecture of the Catalytic Core of the Ectoine Hydroxylase. *J. Mol. Biol.* **2014**, *426*, 586−600.
(31) Zhang, Z.; Gu, Q.; Vasudevan, A. A. J.; Hain, A.; Kloke, B.-P.; Hasheminasab, S.; Mulnaes, D.; Sato, K.; Cichutek, K.; Häussinger, D. Determinants of Fiv and Hiv Vif Sensitivity of Feline Apobec3 Restriction Factors. *Retrovirology* **2016**, *13*, 46.
(32) Milić, D.; Dick, M.; Mulnaes, D.; Pfleger, C.; Kinnen, A.; Gohlke, H.; Groth, G. Recognition Motif and Mechanism of Ripening Inhibitory Peptides in Plant Hormone Receptor Etr1. *Sci. Rep.* **2018**, *8*, 3890.
(33) Mulnaes, D.; Gohlke, H. Topscore: Using Deep Neural Networks and Large Diverse Data Sets for Accurate Protein Model Quality Assessment. *J. Chem. Theory Comput.* **2018**, *14*, 6117−6126.
(34) Chovancova, E.; Pavelka, A.; Benes, P.; Strnad, O.; Brezovsky, J.; Kozlikova, B.; Gora, A.; Sustr, V.; Klvana, M.; Medek, P.; Biedermannova, L.; Sochor, J.; Damborsky, J. Caver 3.0: A Tool for the Analysis of Transport Pathways in Dynamic Protein Structures. *PLoS Comput. Biol.* **2012**, *8*, No. e1002708.
(35) Salomon-Ferrer, R.; Götz, A. W.; Poole, D.; Le Grand, S.; Walker, R. C. Routine Microsecond Molecular Dynamics Simulations with Amber on Gpus. 2. Explicit Solvent Particle Mesh Ewald. *J. Chem. Theory Comput.* **2013**, *9*, 3878−3888.
(36) Case, D. A.; I.Y. Ben-Shalom, S. R. B.; D.S. Cerutti, T. E.; Cheatham, V. W. D., III; Cruzeiro, T. A.; Darden, R. E.; Duke, D. G. G.; Giambasu, T.; Giese, M. K.; Gilson, H.; Gohlke, A. W.; Goetz, D.; Greene, R.; Harris, N.; Homeyer, Y. H. S.; Izadi, A.; Kovalenko, R.; Krasny, T.; Kurtzman, T. S.; Lee, S.; LeGrand, P.; Li, C.; Lin, J.; Liu, T. L. R.; Luo, V.; Man, D. J.; Mermelstein, K. M.; Merz, Y.; Miao, G.; Monard, C.; Nguyen, H.; Nguyen, A. O. F.; Pan, R.; Qi, D. R.; Roe, A.; Roitberg, C.; Sagui, S.; Schott-Verdugo, J.; Shen, C. L.; Simmerling, J. S.; J. Swails, R. C.; Walker, J.; Wang, H.; Wei, L.; Wilson, R. M.; Wolf, X.; Wu, L.; Xiao, Y.; Xiong, D. M. Y. a. P. A. K. *Amber 2019*; University of California: San Francisco, 2019.
(37) Hopkins, C. W.; Le Grand, S.; Walker, R. C.; Roitberg, A. E. Long-Time-Step Molecular Dynamics through Hydrogen Mass Repartitioning. *J. Chem. Theory Comput.* **2015**, *11*, 1864−1874.
(38) Jacobs, D. J.; Rader, A. J.; Kuhn, L. A.; Thorpe, M. F. Protein Flexibility Predictions Using Graph Theory. *Proteins* **2001**, *44*, 150−165.
(39) Hespenheide, B. M.; Jacobs, D. J.; Thorpe, M. F. Structural Rigidity in the Capsid Assembly of Cowpea Chlorotic Mottle Virus. *J. Condens. Matter Phys.* **2004**, *16*, S5055.
(40) Jacobs, D. J.; Thorpe, M. F. Generic Rigidity Percolation: The Pebble Game. *Phys. Rev. Lett.* **1995**, *75*, 4051.
(41) Rader, A. J.; Hespenheide, B. M.; Kuhn, L. A.; Thorpe, M. F. Protein Unfolding: Rigidity Lost. *Proc. Natl. Acad. Sci. U. S. A.* **2002**, *99*, 3540−3545.
(42) Livesay, D. R.; Jacobs, D. J. Conserved Quantitative Stability/Flexibility Relationships (Qsfr) in an Orthologous Rnase H Pair. *Proteins* **2006**, *62*, 130−143.
(43) Radestock, S.; Gohlke, H. Protein Rigidity and Thermophilic Adaptation. *Proteins* **2011**, *79*, 1089−1108.
(44) Pfleger, C.; Gohlke, H. Efficient and Robust Analysis of Biomacromolecular Flexibility Using Ensembles of Network Topologies Based on Fuzzy Noncovalent Constraints. *Structure* **2013**, *21*, 1725−1734.
(45) Pfleger, C.; Radestock, S.; Schmidt, E.; Gohlke, H. Global and Local Indices for Characterizing Biomolecular Flexibility and Rigidity. *J. Comput. Chem.* **2013**, *34*, 220−233.
(46) Rathi, P. C.; Radestock, S.; Gohlke, H. Thermostabilizing Mutations Preferentially Occur at Structural Weak Spots with a High Mutation Ratio. *J. Biotechnol.* **2012**, *159*, 135−144.
(47) Rathi, P. C.; Jaeger, K.-E.; Gohlke, H. Structural Rigidity and Protein Thermostability in Variants of Lipase a from Bacillus Subtilis. *PLoS One* **2015**, *10*, No. e0130289.
(48) Dick, M.; Weiergräber, O. H.; Classen, T.; Bisterfeld, C.; Bramski, J.; Gohlke, H.; Pietruszka, J. Trading Off Stability against Activity in Extremophilic Aldolases. *Sci. Rep.* **2016**, *6*, 17908.
(49) Rathi, P. C.; Fulton, A.; Jaeger, K.-E.; Gohlke, H. Application of Rigidity Theory to the Thermostabilization of Lipase a from Bacillus Subtilis. *PLoS Comput. Biol.* **2016**, *12*, No. e1004754.
(50) Nutschel, C.; Fulton, A.; Zimmermann, O.; Schwaneberg, U.; Jaeger, K.-E.; Gohlke, H. Systematically Scrutinizing the Impact of Substitution Sites on Thermostability and Detergent Tolerance for Bacillus Subtilis Lipase A. *J. Chem. Inf. Model.* **2020**, *60*, 1568−1584.
(51) Gohlke, H.; Kuhn, L. A.; Case, D. A. Change in Protein Flexibility Upon Complex Formation: Analysis of Ras-Raf Using Molecular Dynamics and a Molecular Framework Approach. *Proteins* **2004**, *56*, 322−337.
(52) Alonso, S.; Santiago, G.; Cea-Rama, I.; Fernandez-Lopez, L.; Coscolín, C.; Modregger, J.; Ressmann, A. K.; Martínez-Martínez, M.; Marrero, H.; Bargiela, R.; Pita, M.; Gonzalez-Alfonso, J. L.; Briand, M. L.; Rojo, D.; Barbas, C.; Plou, F. J.; Golyshin, P. N.; Shahgaldian, P.; Sanz-Aparicio, J.; Guallar, V.; Ferrer, M. Genetically Engineered Proteins with Two Active Sites for Enhanced Biocatalysis and Synergistic Chemo- and Biocatalysis. *Nat. Catal.* **2020**, *3*, 319−328.
(53) Eisenthal, R.; Danson, M. J.; Hough, D. W. Catalytic Efficiency and Kcat/Km: A Useful Comparator? *Trends Biotechnol.* **2007**, *25*, 247−249.
(54) Nath, A.; Atkins, W. M. A Quantitative Index of Substrate Promiscuity. *Biochemistry* **2008**, *47*, 157−166.
(55) Hawkins, P. C. D.; Skillman, A. G.; Nicholls, A. Comparison of Shape-Matching and Docking as Virtual Screening Tools. *J. Med. Chem.* **2007**, *50*, 74−82.
(56) Arpigny, J. L.; Jaeger, K.-E. Bacterial Lipolytic Enzymes: Classification and Properties. *Biochem. J.* **1999**, *343*, 177−183.
(57) Mariani, V.; Biasini, M.; Barbato, A.; Schwede, T. Lddt: A Local Superposition-Free Score for Comparing Protein Structures and Models Using Distance Difference Tests. *Bioinformatics* **2013**, *29*, 2722−2728.
(58) Greenfield, N. J. Using Circular Dichroism Collected as a Function of Temperature to Determine the Thermodynamics of Protein Unfolding and Binding Interactions. *Nat. Protoc.* **2006**, *1*, 2527−2535.
(59) Mayr, H.; Ofial, A. R. The Reactivity−Selectivity Principle: An Imperishable Myth in Organic Chemistry. *Angew. Chem. Int. Ed. Engl.* **2006**, *45*, 1844−1854.
(60) Wells, P. R. Linear Free Energy Relationships. *Chem. Rev.* **1963**, *63*, 171−219.
(61) Böhm, H.-J. The Development of a Simple Empirical Scoring Function to Estimate the Binding Constant for a Protein-Ligand

Complex of Known Three-Dimensional Structure. *J. Comput.-Aided Mol. Des.* **1994**, *8*, 243−256.
(62) Feig, M. Computational Protein Structure Refinement: Almost There, yet Still So Far to Go. *Wiley Interdiscip Rev Comput Mol Sci* **2017**, *7*, e1307.
(63) Heo, L.; Feig, M. Experimental Accuracy in Protein Structure Refinement Via Molecular Dynamics Simulations. *Proc. Natl. Acad. Sci. U. S. A.* **2018**, *115*, 13276−13281.
(64) Heo, L.; Arbour, C. F.; Feig, M. Driven to near-Experimental Accuracy by Refinement Via Molecular Dynamics Simulations. *Proteins* **2019**, *87*, 1263−1275.
(65) Müller, H.; Becker, A. K.; Palm, G. J.; Berndt, L.; Badenhorst, C. P. S.; Godehard, S. P.; Reisky, L.; Lammers, M.; Bornscheuer, U. T. Sequence-Based Prediction of Promiscuous Acyltransferase Activity in Hydrolases. *Angew Chem Int Ed Engl* **2020**, *59*, 11607−11612.
(66) Seibert, C. M.; Raushel, F. M. Structural and Catalytic Diversity within the Amidohydrolase Superfamily. *Biochemistry* **2005**, *44*, 6383−6391.
(67) Oppermann, U.; Filling, C.; Hult, M.; Shafqat, N.; Wu, X.; Lindh, M.; Shafqat, J.; Nordling, E.; Kallberg, Y.; Persson, B. Short-Chain Dehydrogenases/Reductases (Sdr): The 2002 Update. *Chem.-Biol. Interact.* **2003**, *143-144*, 247−253.
(68) Fushinobu, S.; Nishimasu, H.; Hattori, D.; Song, H.-J.; Wakagi, T. Structural Basis for the Bifunctionality of Fructose-1, 6-Bisphosphate Aldolase/Phosphatase. *Nature* **2011**, *478*, 538−541.
(69) Du, J.; Say, R. F.; Lü, W.; Fuchs, G.; Einsle, O. Active-Site Remodelling in the Bifunctional Fructose-1, 6-Bisphosphate Aldolase/Phosphatase. *Nature* **2011**, *478*, 534−537.
(70) Ovchinnikov, V.; Louveau, J. E.; Barton, J. P.; Karplus, M.; Chakraborty, A. K. Role of Framework Mutations and Antibody Flexibility in the Evolution of Broadly Neutralizing Antibodies. *Elife* **2018**, *7*, e33038.
(71) Stockwell, G. R.; Thornton, J. M. Conformational Diversity of Ligands Bound to Proteins. *J. Mol. Biol.* **2006**, *356*, 928−944.
(72) Perola, E.; Charifson, P. S. Conformational Analysis of Drug-Like Molecules Bound to Proteins: An Extensive Study of Ligand Reorganization Upon Binding. *J. Med. Chem.* **2004**, *47*, 2499−2510.
(73) Krause, D. Juwels: Modular Tier-0/1 Supercomputer at the Jülich Supercomputing Centre. *JLSRF* **2019**, *5*, A135.



https://doi.org/10.1021/acs.jcim.1c00152
*J. Chem. Inf. Model.* 2021, 61, 2383−2395